Desalination and Water Treatment
www.deswater.com

doi: 10.5004/dwt.2022.28319

255 (2022) 34–46
April

Enhancing the value of agro-food waste in the treatment of water laden with organic pollutants

Djeziri Soumia*, Djellouli Hadja Mebarka

Materials & Catalysis Laboratory, Department of Chemistry, Faculty of Exact Sciences, D. LIABES University, BP 89, Sidi Bel-Abbés, Algeria, email: Somiadjeziri22@gmail.com (D. Soumia)

Received 30 June 2021; Accepted 30 January 2022

ABSTRACT

The present study concerns the valorization of an agro alimentary waste, namely: the olive stone, collected at the level of Sidi Bel Abbes (Algeria), in the field of water charged in organic pollutants treatment. The material was used after calcinations process and chemical activation by phosphoric acid to improve its adsorptive capacity. A range of analyses was carried out, for the characterization of the adsorbent used, among them: the infrared spectroscopy, iodine index, moisture content and ash content. In order to test the performance of activated carbon this is concerned in organic pollutants and in particular phenol considered as very toxic pollutant. The effect of several parameters such as contact time, initial concentration, pH of the solution and temperature were studied. All the results obtained show that the adsorption kinetics of phenol on prepared activated carbon is well described by the pseudo-second-order. The adsorption isotherms of the studied adsorbent/adsorbate systems are satisfactorily described by the Temkin model. On the other hand, the thermodynamic study revealed that the adsorption is exothermic of physisorption type. The obtained results demonstrate the possibility of olive pits valorization in the form of activated carbon with what all this implies as socio-economic impacts.

Keywords: Adsorption; Activated carbon; Olive stones; Phenol

1. Introduction

Nowadays, the increasing request for adsorbent materials for environmental protection processes is leading to further research in the manufacture of activated carbons from non-conventional materials, in particular from vegetable waste.

The raw materials used as precursors are of various origins: (i) Lignocellulosic derivatives (wood, coconut shells, almond, hazelnut and walnut shells, apricot pits, apple pulp, peach pits as well as olive pits, date pits…). (ii) Polymers, as well as mineral carbons [1].

The elaboration of activated carbons from vegetable wastes is however very interesting throughout the economic point of view because we are taking profits from simple transformations, from a direct application of these starting materials [2]. Many scientists from different disciplines are increasingly interested in the identification and elimination of environmental pollutants or toxic substances that cause morbidity and mortality in humans or animals. For this purpose, adsorption on activated carbon is often used, in particular for the elimination of toxic substances, organic or inorganic micro pollutants from water, the discoloration of vegetable oils and the purification of numerous products (juice, sugar syrup, wine, beer, etc.) [3].

The main objective of this work is devoted, firstly, to the preparation of an activated carbon from agro alimentary waste, olive stones, then we characterized it by several methods. Second, we studied the adsorption of a model organic compound, phenol, on the prepared activated carbon.

* Corresponding author.

Presented at the International Virtual Conference on Water and Energy (ICWE 21), Hassiba Benbouali University of Chlef, Algeria, 25–27 May 2021

1944-3994/1944-3986 © 2022 Desalination Publications. All rights reserved.

2. Materials and methods

2.1. Preparation of activated carbon from olive stones

The olive stones used in this study were collected in the region of Sidi Bel Abbes. The following protocol allows obtaining the activated carbon from the olive stones.

2.1.1. Purification

The olive stones are washed several times with running water to remove adhering impurities and dust, as well as water-soluble substances, until a fairly clear washwater is obtained [4]. After washing, the cores are dried for 24 h at a temperature of 110°C in an oven and then crushed with an electric grinder and sieved to obtain a powder.

2.1.2. Carbonization

After drying, the raw material is carbonized at the precise temperature 400°C for 1 h in a muffle furnace (Nabertherm).

2.1.3. Activation

Once the stones are calcined at 400°C, they underwent a chemical activation. The activating agent used was an acid (H_3PO_4). Indeed, this agent has been widely used for the activation of carbons [5]. For the activation, 20 g of calcined olive stones were dispersed in a volume of a phosphoric acid solution (1N) under electromagnetic stirring. The contact time initially set at 3 h. The impregnated adsorbents are separated by simple filtration. Then the mixture is put in the oven for 1 h at 110°C.

2.1.4. Washing and drying

After cooling, the prepared activated carbon was cleaned several times with distilled water in order to reach a neutral pH [6]. The last step is the drying of the prepared adsorbent at 110°C, for 24 h, until constant weight is obtained. The obtained activated carbon was stored in boxes for its use.

2.2. Characterization of prepared activated carbon

The knowledge of these characteristics is necessary to identify the efficiency of our material.

2.2.1. Moisture content

The moisture content represents the amount of water physically not bound to the activated carbon. Moisture is a ratio expressed as a percentage, it is determined by drying the adsorbent in an oven at 105°C until its weight remains constant, it is calculated by the following relationship [4]:

$$H\% = \frac{m_0 - m_1}{m_0} \times 100 \quad (1)$$

where H: moisture in mass percentage (%), m_0: mass of adsorbent before drying (g), m_1: mass of adsorbent after drying (g).

2.2.2. Ash rate

This is the inorganic, inert, amorphous and unusable part present in the material [6]. A 1 g sample of adsorbent is placed in a crucible. This crucible is introduced into the oven and we heated for 1 h up to 1,000°C. After cooling, we weighed the crucible. The ash content is calculated by the following formula [4]:

$$\%\text{Ash} = \frac{p_0 - p_1}{p_0} \times 100 \quad (2)$$

where p_0: weight of the filled crucible before carbonization in (g); p_1: weight of the crucible filled after carbonization in (g).

2.2.3. Iodine value

The iodine index (iodine number) is a microspore content measure of an adsorbent material. The iodine number is an indicator of the porosity of an activated carbon [7]. The iodine adsorption capacity of each material was determined according to the following procedure: 10 mL of a 0.01 N iodine solution in an Erlenmeyer flask and we dosed with a 0.1 N sodium thiosulfate solution, in a few drops presence of a starch solution as indicator until the color disappeared. The reading volume corresponds to V_b. 0.05 g of activated carbon to an Erlenmeyer flask containing 15 mL of a 0.1 N iodine solution with stirring for 5 min. afterwards; we filtered and assayed the iodine of 10 mL filtrate by 0.1 N sodium thiosulfate solution in the presence two drops presence of a starch solution [8].

The iodine value is calculated by the following formula:

$$\text{Id} = \frac{\left(V_b - V_s\right) \cdot N \cdot \left(126.9\right) \cdot 15/10}{M} \quad (3)$$

where $(V_b - V_s)$: difference of the blank and adsorbent titration results in (mL of 0.1 N sodium thiosulfate); N: normality of the sodium thiosulfate solution in (mol/L); 126.9: the atomic mass of iodine; M: the mass of the adsorbent in (g).

The results of moisture analysis, ash content and iodine index of raw material, both calcined materials and activated carbons are shown in Table 1.

2.2.3.1. Discussion of results

From our results, we noticed that the ash content of the materials: crude, calcined and prepared activated carbon represent a low content of mineral matter (ash).

These materials also have low moisture content; this finding highlights a low retention of water content [8]. For the iodine value, the results vary according to the calcination and the activation used (activating agent). The prepared activated carbon gives a good iodine value with a value of 1,104.03 mg/g which was high compared to the value found by Haimour and Emeish [9].

In fact, according to the literature, the moisture content and the ash content must be low for excellent adsorbents. And for activated carbons that have an iodine index

Table 1
Moisture, ash content and iodine value of raw material, olive stones calcined at 400°C and prepared activated carbon

Sample	Moisture content (%)	Ash rate (%)	Iodine value (mg/g)
Olive stones	0.13	0.92	799.47
Calcined olive stones at 400°C	0.0155	3.81	1,080.17
Activated carbon	0.0287	1.424	1,104.03

greater than 950 mg/g have a power of adsorption of small molecules [8].

2.2.4. Structural analysis by Fourier-transform infrared spectroscopy

The analysis of materials by infrared spectroscopy (IR) was carried out at the materials and catalysis Laboratory of Sidi Bel Abbes University (Algeria), in order to identify the functional groups [10] present on the surface of the latter. This analysis was conducted on an infrared spectroscopy apparatus of Fourier-transform infrared spectroscopy (FTIR) type. The analysis was done on a range of wave numbers from 650–4,000 cm^{-1}. The infrared spectra of the different adsorbents: raw materials olive stone; calcined olive stones at 400°C and the prepared activated carbon are shown in Figs. 1–3.

We have gathered the interpretation of the spectra in Table 2.

2.2.4.1. Discussions

The broadband of 3,347.78 cm^{-1} corresponding to the hydrogen valence vibration of the O–H hydroxyl groups (of carboxyls, phenols or alcohols) is only found in the spectrum of olive stones. These functions are totally absent in the spectrum of calcined olive stones. This band is also absent in the spectrum of activated carbon.

For the bands from 2,855.2 to 2,991.4 cm^{-1} and 1,371.5 to 1,409.2 cm^{-1} which correspond to the C–H elongation vibration of the aliphatic molecules [12] of the aromatic rings and to the C–H bond deformation vibration of the methyl and methylene groups successively are much weaker for calcined stones at 400°C and activated charcoal with a variation of the intensity. We observed a small decrease in the intensity of the peaks 1,735.65 cm^{-1} for calcined and chemically activated olive cores comparable with crude olive cores, this is due to the carbonization and activation for the bands that correspond to the C=C bonds appear in the spectrum of raw olive cores with several neighboring peaks and almost the same intensity. After carbonization followed by activation, we noticed a decrease in the number of peaks with a variation in intensity.

The vibration band peak 1,031.30 cm^{-1} which represents the valence phenols vibration of C–O bonds, carboxylic acid, alcohol and ester is very intense (strong) for the raw olive core spectrum but after carbonization, the intensity is decreased(weak) and same for the activated charcoal. Finally, the bands from 742.49 to 893.6 cm^{-1} of out-of-plane deformation vibration CH in aromatic rings are present in all spectra with a variation of intensity.

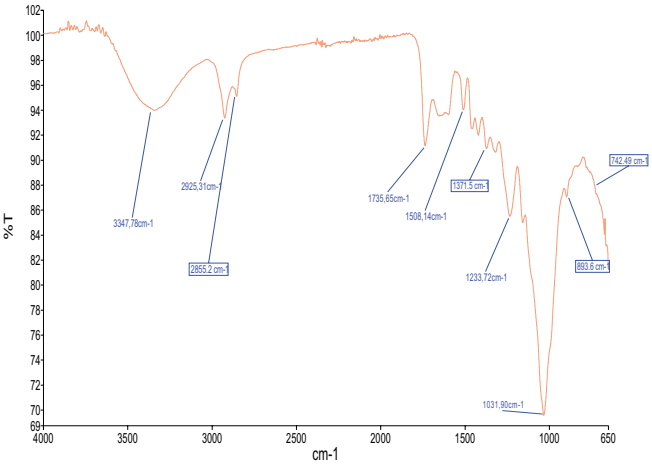

Fig. 1. IR spectra of raw olive stones.

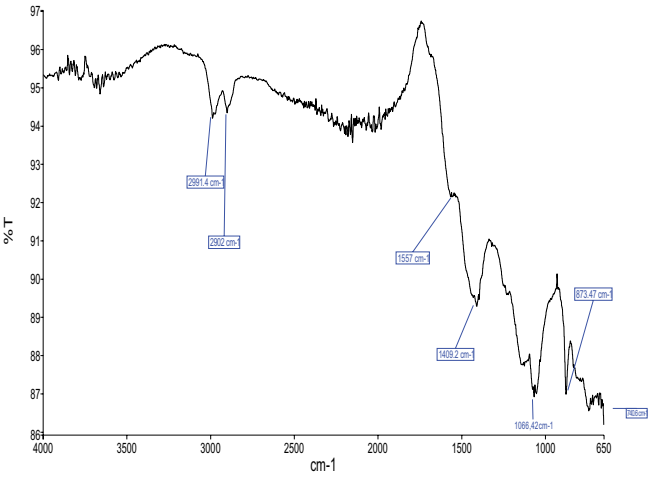

Fig. 2. IR spectra of calcined olive stones at 400°C.

3. Results and discussion

In this last part, we approach the study of an activated adsorption phenomenon carbon synthesized based on olive rings to purify aqueous solutions containing phenol. In a first step, we studied the influence of different parameters on the adsorption capacity: the mass of adsorbent, the contact time, the pH of the solution, the temperature and the concentration of the adsorbed molecule. Afterwards, we tried to apply different kinetic laws such as the pseudo-first-order, pseudo-second-order, Elovich velocity equations and the intra-particle and external diffusion

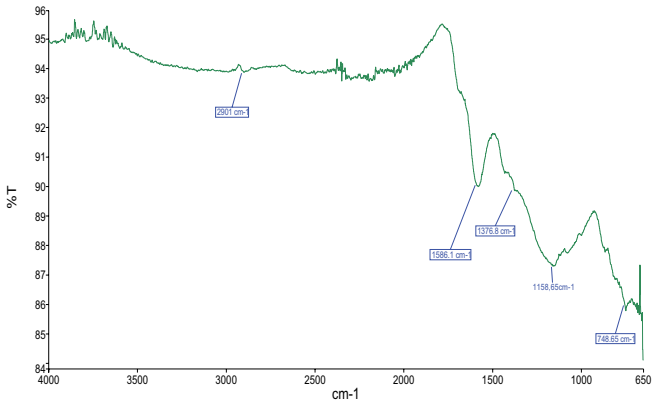

Fig. 3. IR spectra of the prepared activated carbon.

model to simulate the pollutants experimental data of adsorption kinetics. Then, we started to apply the thermodynamic relations to calculate the thermodynamic quantities and determine the type of adsorption. Finally, we studied the adsorption isotherms whose parameters express the surface properties and the affinity of the adsorbent.

3.1. Phenol analysis

Before studying the phenol phenomenon of adsorption, we must first determine its maximum wavelength λ_{max} and verify the validity of the Beer–Lambert law for the concentration range studied.

3.1.1. Wavelength determination of the absorption maximum λ_{max}

We prepared solutions of phenol with concentrations between 1 and 100 mg/L. And we measured the wavelengths λ between 200 and 300 nm with a Perkin-Elmer UV/VIS Spectrometer Lambda. The maximum absorption wavelength (λ_{max}) for phenol is at 269.93 nm, as shown in Fig. 4.

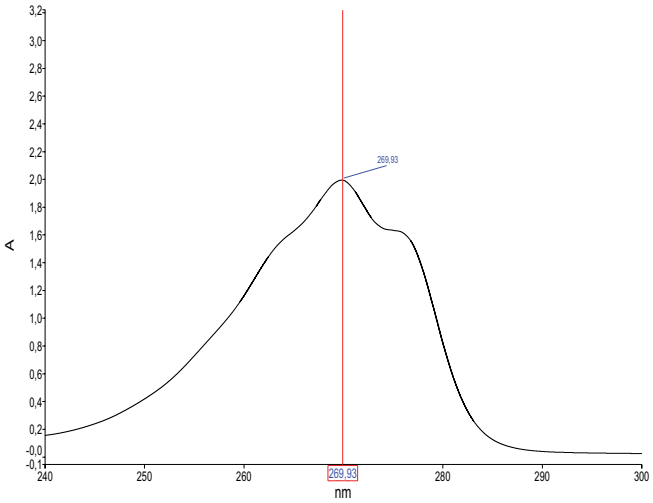

Fig. 4. Scanning phenol curve.

3.1.2. Calibration curve (Application of the Beer–Lambert law)

The calibration curve is obtained by expressing the variation of the absorbance as a function of phenol concentration $A = f(c)$ Beer–Lambert's law: When a monochromatic radiation beam of intensity I_0 crosses a colored substance, an absorption of energy takes place so that the intensity of the emerging incident beam I is lower. This monochromatic absorption follows the Beer–Lambert law which is expressed as follows [16]:

$$A = \varepsilon lC \tag{4}$$

where A is the absorbance at a wavelength λ (without unit); ε is the molar extinction coefficient, expressed in L/mol cm; l is the thickness of the cell (in cm); C: is the molar concentration of the solution (in mol/L).

Table 2
Interpretations of the infrared bands observed in the FTIR spectra of different materials

Vibration bands	Interpretations of bands
3,347.78 cm^{-1}	Represents a broadband with an average intensity corresponding to the hydrogen valence vibration of O–H hydroxyl groups (of carboxyls, phenols or alcohols) [11].
2,855.2–2,991.4 cm^{-1}	Represents the C–H elongation vibration of aliphatic molecules [12] of aromatic rings [13] with thin bands of medium intensities.
1,735.65 cm^{-1}	Represents a thin band with an average intensity corresponding to the vibration of elongation at C=O bonds of carbonyl functions (ketones; aldehydes; carboxylic acids) [12].
1,508.14–1,586.1 cm^{-1}	Represents the elongation vibration of C=C bonds [12] of aromatic rings [13] and [14] with low band intensity.
1,371.5–1,409.2 cm^{-1}	Represents a thin band with an average intensity which corresponds to the vibration of the deformation of the C–H bonds of the methyl and methylene groups [12].
1,031.9–1,233.72 cm^{-1}	Represents different bands (weak and strong) corresponding to the valence vibration [15] of the C–O bonds of phenols, carboxylic acid, alcohol and ester [12].
742.49–893.6 cm^{-1}	Are due to the out-of-plane deformation mode of C–H in aromatic rings [11] with thin bands and moderately strong intensity.

The experimental data reported in Fig. 5 indicate the linear relationship between absorbance and concentration with a high regression coefficient (R^2 = 0.998).

The unknown phenol concentration determined from the application of Beer–Lambert law. $A = 0.01449C$.

3.2. Parameters optimization

We calculated the adsorption yield by the following formula [17]:

$$R\% = \frac{c_0 - c_t}{c_0} \times 100 \quad (5)$$

where $R\%$: adsorption efficiency, c_0 = initial concentration of adsorbate and c_t = final concentration of the adsorbate after the time.

3.2.1. Mass influence

The effect of activated carbon mass on phenol adsorption is shown in Fig. 6, we varied the mass of activated carbon from 0.2 to 2.5 g, the concentration of phenol is 100 mg/L at a room temperature, and the contact time is 60 min.

Fig. 6 gives us the percentage of phenol adsorption as a function of the adsorbent mass. This figure shows that in all cases, the percentage of this pollutant removal increases when the mass of the adsorbent increases until total saturation. This is easily understandable, because the increase in the mass of the adsorbent increases the specific surface and thus the number of available adsorption sites [16]. The curve in Fig. 6 shows that 1.5 g of carbon mass is able to bind a maximum of phenol. For this, we will continue our experimental work by fixing the optimal mass of activated carbon which is equal to 1.5 g.

3.2.2. Influence of contact time

To study the kinetics of adsorption on activated carbon from olive pits, a volume of phenol solution about 100 mL (100 mg/L) is mixed with 1.5 g of adsorbent mass. The whole is stirred for different contact times varying from 5 to 120 min at room temperature.

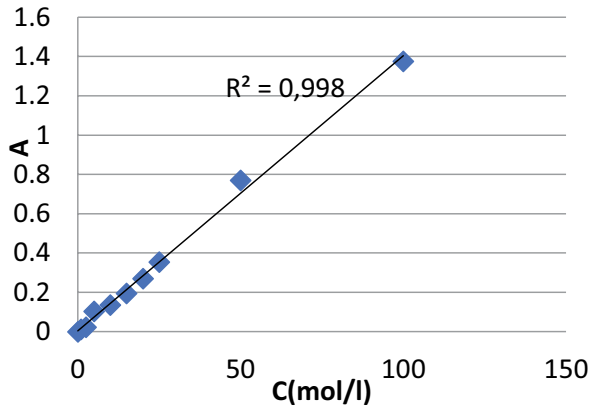

Fig. 5. Calibration curve for phenol.

Fig. 7 represents the variation of phenol adsorption as a function of time. This figure shows that the adsorption phenol capacity increases as a function of contact time until reaching a saturation level. The evolution of the phenol adsorption process as a function of time shows that the equilibrium is established after 60 min, from this contact time all the adsorption sites become occupied. According to this result, we will continue the phenomenon study adsorption by fixing the contact time at 60 min.

3.2.3. pH influence

For a given carbon, the nature of the interactions and the adsorption capacity will be modified according to the pH value. The pH is one of the most important parameters to be taken into account during an adsorption process because it affects both the external charge of the adsorbent and the degree of the adsorbate ionization [4]. To study the

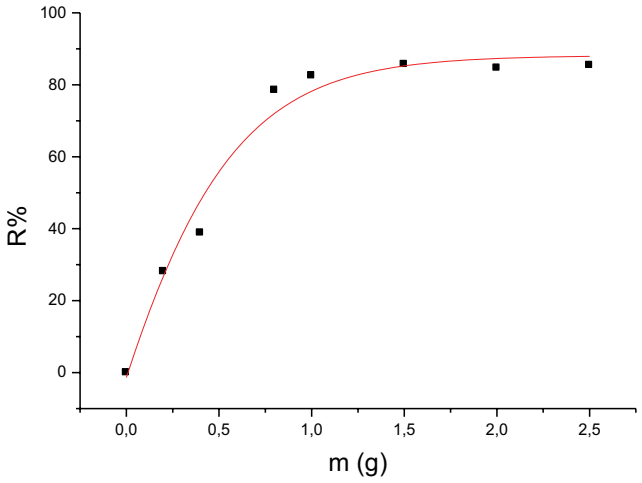

Fig. 6. Effect of activated carbon mass on phenol adsorption (t = 1 h, V = 100 mL, pH phenol = 6.3, C = 100 mg/L).

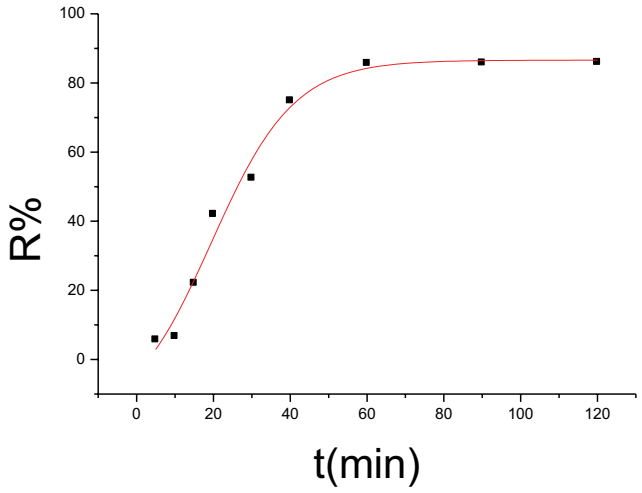

Fig. 7. Time effect of activated carbon on phenol adsorption (m = 1.5 g, V = 100 mL, pH phenol = 6.3, C = 100 mg/L).

pH influence on the adsorption of phenol by activated carbon prepared using 100 mL concentration solution 100 mg/L for different pH, at room temperature and contact time of 60 min, the activated carbon amount used is 1.5 g. The results are shown in Fig. 8.

From Fig. 8, we observe a decrease of phenol removal percentage when the solution pH increases. When the pH of the solution is acidic, the adsorption efficiency is very high, and we notice that there is a maximum of 92.85% adsorption for pH = 1.83. According to these results, the pH = 1.83 is considered as an optimal pH.

3.2.4. Temperature influence

The influence of temperature was studied with phenols solutions (100 mL) at pH = 1.83, immersed in a thermostatically controlled water bath to keep the desired temperature constant, the values of temperatures studied were 20°C, 50°C, 60°C, 65°C and 75°C. The contact time is 60 min.

From the results given in Fig. 9, we can deduce the following: The adsorption of phenol is maximum at 20°C; it reaches a removal rate of 92.85%. The amount of phenol adsorbed decreases as the temperature increases, it is therefore favored at low temperature which shows that the process is exothermic and we can admit that it is a physisorption [18].

3.2.5. Influence of concentration

The tests were carried out by stirring 1.5 g of the adsorbent for 60 min in phenol solutions with concentrations ranging from 25 to 350 mg/L. The tests were performed at acidic pH (1.83) at room temperature. The residual concentrations were determined and then evaluated to follow the evolution of the quantity adsorbed per unit mass as a function of the initial concentration (Fig. 10). The residual concentration of adsorbed impurities is measured using the following equation [19]:

$$q_e = \frac{C_0 - C_e}{M} V \tag{6}$$

where q_e: amount of adsorbed solute (mg/g); V: volume of solution (l); C_0: mass concentration of solute (mg/L); C_e: residual [19] concentration of solute at adsorption equilibrium (mg/L); M: mass of adsorbent used (g) [13].

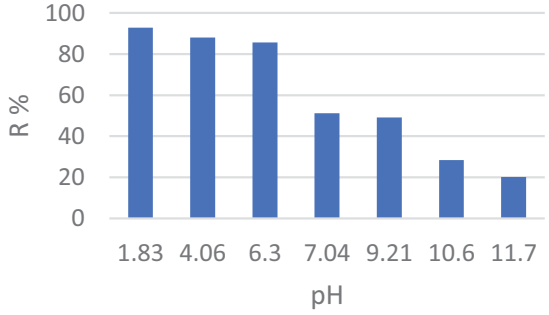

Fig. 8. Effect of activated carbon pH on phenol adsorption (m = 1.5 g, V phenol = 100 mL, t = 60 min, C phenol = 100 mg/L).

Fig. 10 represents the variation of the adsorbed phenol amount as a function of its initial concentration. The results show that the adsorption capacity of phenol increases with its initial concentration increase.

3.3. Modeling of adsorption kinetics

Several kinetic models were used to interpret the experimental data, to give essential information for the use of these activated carbons in the adsorption field. We have adopted five kinetic models.

These models are: pseudo-first-order, pseudo-second-order, Elovich and intraparticle diffusion and external diffusion models.

3.3.1. Intraparticle diffusion

Described by the model of Weber and Morris (1963) [15,18]:

$$q_t = K_i \cdot t^{1/2} + C \tag{7}$$

where K_i: velocity constant of intraparticle diffusion (mg/g min$^{1/2}$); C: the intersection of the line with the y-axis: in

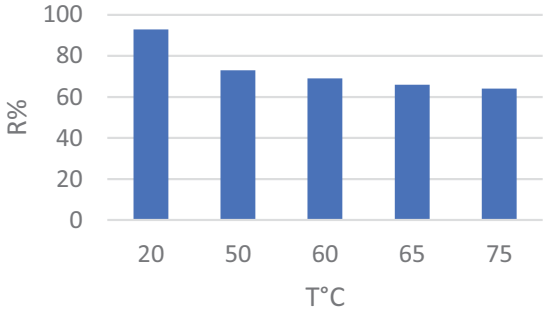

Fig. 9. Temperature effect of activated carbon on phenol adsorption (t = 1 h, V = 100 mL, m = 1.5 g, C = 100 mg/L, pH = 1.83).

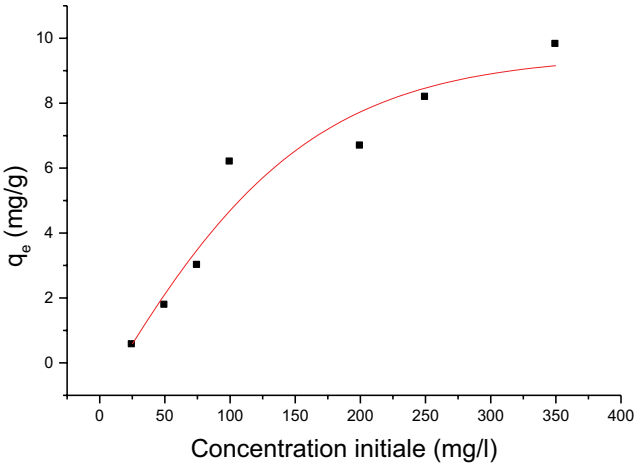

Fig. 10. Effect of initial activated carbon concentration on phenol adsorption (t = 1 h, V = 100 mL, pH phenol = 1.83, m = 1.5 g).

the case where the value of C is zero, intra-granular diffusion is the limiting step in the adsorption kinetics [18,20].

Fig. 11 shows the linear form of this equation that was described previously which means the q_t trace as a function of $t^{1/2}$ [18].

3.3.2. External diffusion step

In 2007, Bhattacharyya and Cupta proposed the model [18]:

$$\ln\left(1-\frac{q_t}{q_e}\right)=-k_{fd}\cdot t+C \tag{8}$$

where q_t: amount of solute adsorbed per unit mass of adsorbent at time t (mg/g), k_{fd}: diffusion rate constant in the liquid film (min^{-1}). C: constant: the smaller the value of C, the more the extra-granular diffusion governs the adsorption process. In the case where C is null, the extra-granular diffusion is the limiting step of the adsorption kinetics [18].

We have plotted $\ln(1-q_t/q_e)$ as a function of time in Fig. 12.

3.3.3. Surface reaction step

The expressions found most often in the bibliography.

3.3.3.1. Expression of Lagergren pseudo-first-order (1898) [18]

$$\ln\left(q_e-q_t\right)=\ln\left(q_e\right)-k_1\cdot t \tag{9}$$

where k_1: pseudo-first-order rate constant (min^{-1}).

The plot of $\ln(q_e-q_t)$ vs. time is shown in Fig. 13.

3.3.3.2. Expression of the pseudo-second-order very often used [18]

$$\frac{1}{q_t}=\frac{1}{k_2q_{e2}\cdot t}+\frac{1}{q_e} \tag{10}$$

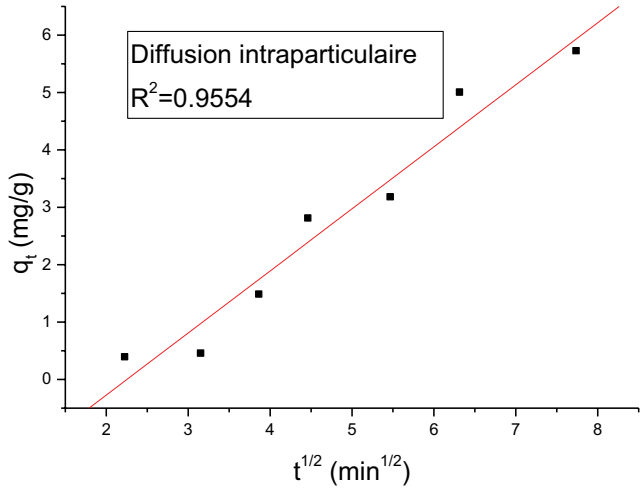

Fig. 11. Graphical representation of the kinetic modeling, the intraparticle diffusion model.

where k_2: rate constant of pseudo-second-order (g/mg min). Fig. 14 shows inverse variation of adsorbed quantity according to inverse of time.

3.3.3.3. Elovich model

It can be expressed as:

$$q_t=\frac{\ln\left(\alpha_E\cdot\beta_E\right)}{\beta_E}+\frac{1}{\beta_E}\ln t \tag{11}$$

where α: the initial adsorption rate (mg/g min) and β: the desorption constant (g/mg min). Using a simple graph $q_t=f(\ln t)$ which is shown in Fig. 15, we have determined the values of α and β.

3.3.3.4. Calculation and model constants

The constants of each model are grouped in Table 3.

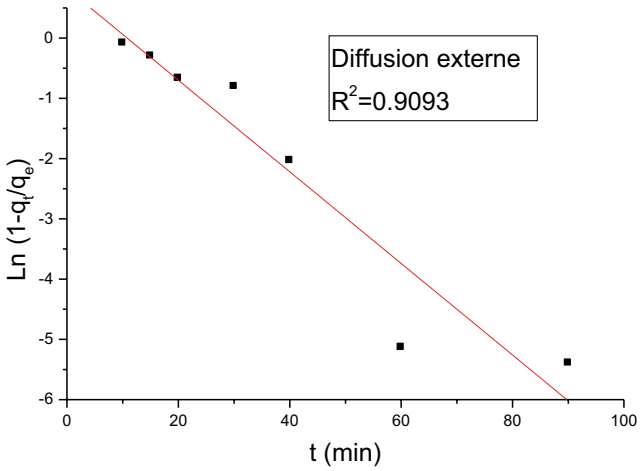

Fig. 12. Graphical representation of the kinetic modeling, the external diffusion model.

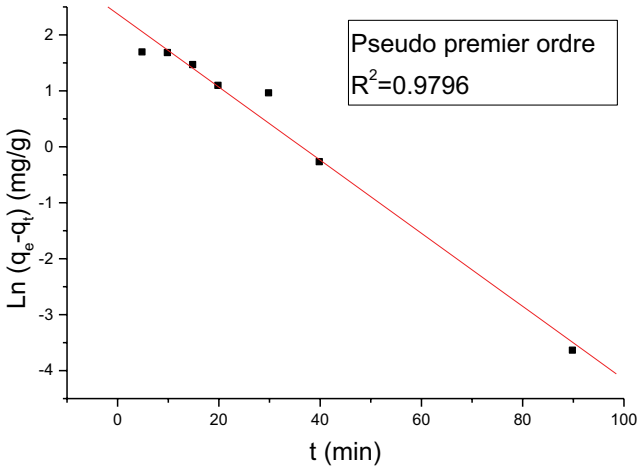

Fig. 13. Graphical representation of the kinetic modeling, the pseudo-first-order model.

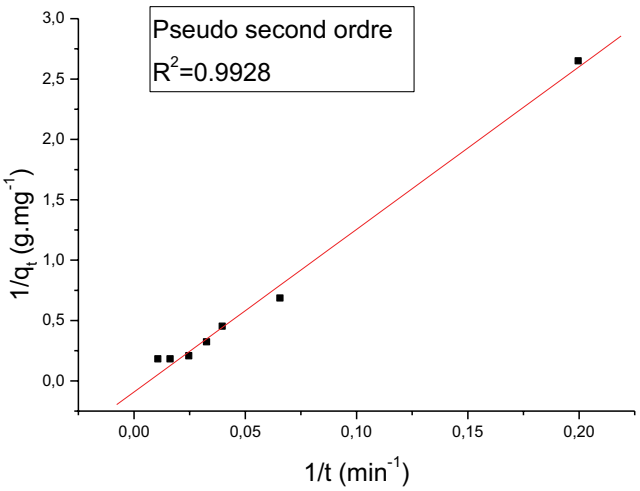

Fig. 14. Kinetic modeling graphical representation of pseudo-second-order model.

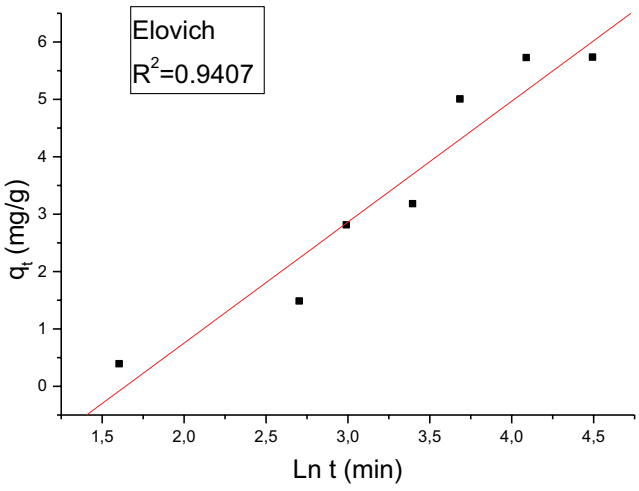

Fig. 15. Kinetic modeling graphical representation, model of Elovich.

The validity of kinetic adsorption model is examined from the R^2 value of the correlation coefficient, the higher this factor the more favorable the model is for the adsorption study process [4]. From the results grouped in Table 3, all the kinetic models have very large regression coefficient values ($R^2 > 0.90$), but the pseudo-second-order model has a higher correlation coefficient value ($R^2 = 0.9928$) than the other models, so we can deduce that the pseudo-second-order model is the one that better describes the adsorption process of phenol on the prepared activated carbon. Also, the value of the adsorbed quantity calculated by the kinetic model of pseudo-second-order is very close to the value of experimental adsorbed quantity.

3.4. Thermodynamic quantities

In order to confirm the previous findings, we proceeded to the determination of the thermodynamic parameters of this process in the studied temperature range such as the standard free enthalpy $\Delta G°$, the standard enthalpy $\Delta H°$ and the standard entropy $\Delta S°$ which were determined using the following equations [21–23]:

$$K_d = \frac{Q_e}{C_e} \tag{12}$$

$$\Delta G° = -\Delta H - T\Delta S° = -RT\ln K_d \tag{13}$$

$$\ln K_d = \frac{\Delta S}{R} - \frac{\Delta H}{R}\frac{1}{R} \tag{14}$$

where K_d: distribution constant, Q_e: adsorbed quantity at equilibrium (mg/g), C_e: equilibrium concentration of the solute (mg/L), $\Delta H°$: enthalpy (kJ/mol), $\Delta S°$: entropy (kJ/mol), $\Delta G°$; free enthalpy (kJ/mol), R: constant of perfect gases (8.314 J/mol K [24]) and T: absolute temperature (K).

By exploiting the data provided by the linear regression of the curve presented in Fig. 16.

Table 3
Constants of kinetic models

Kinetic models	Constants	Prepared activated carbon
Intraparticle diffusion	K_i (mg/g min$^{1/2}$)	1.08161
	R^2	0.9554
Diffusion step	K_F (min^{-1})	0.076
	R^2	0.9093
Pseudo-first-order	k_1 (min^{-1})	0.0653
	q_e (mg/g)	10.735
	R^2	0.9796
Pseudo-second-order	k_2 (min^{-1})	0.000729
	q_e (mg/g)	5.99
	R^2	0.9928
Elovich	α_E (mg/g min)	0.406
	β_E (g/mg min)	0.475
	R^2	0.9267

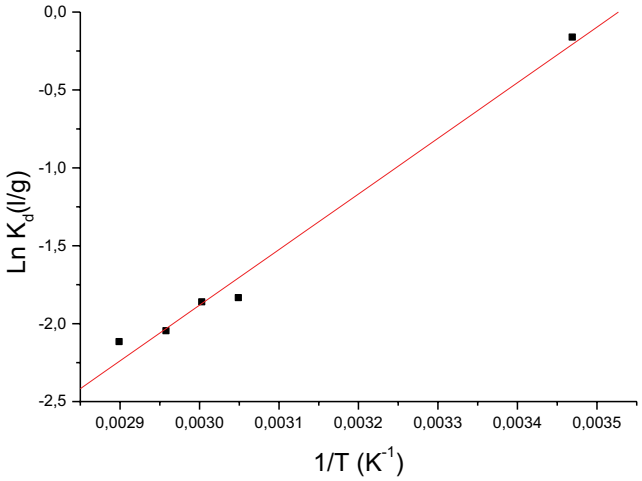

Fig. 16. Phenol influence of the temperature on the adsorption.

According to the graph, there is a line with an interesting regression coefficient (R^2 = 0.987).

The values of the thermodynamic parameters are grouped in Table 4.

The enthalpy $\Delta H°$ is negative, which implies that the process of adsorption is exothermic [21,25]. We also noticed that $\Delta G°$ increases with the increase of the solution temperature, which can be explained by the fact that the adsorption becomes very difficult and disadvantaged when the temperature becomes very large [4] [23]. The phenol adsorption process is of physical adsorption type since the enthalpy value is less than 40 kJ/mol [26]. The negative value of $\Delta S°$ indicates that there is a decrease in disorder in the solid/solute interface solution system during the adsorption process [21,27].

3.5. Adsorption isotherms

Adsorption isotherms are often exploited for the determination of the maximum binding capacities of pollutants and for the identification type of adsorption (physical or chemical). The equilibrium behavior of sorbents can be elucidated by isothermal adsorption models [28]. The results treated according to the mathematical models of Langmuir and Freundlich, Elovich, Temkin, Dubinin–Radushkevich, Kiselev, Fowler–Guggenheim, Hill de Boer allowed us to calculate the maximum capacity of adsorption as well as the parameters 14 of adsorption [4].

3.5.1. Isotherm of Freundlich

$$q_e = K_F C_e^{1/n} \tag{15}$$

$$\log\left(q_e\right) = \log\left(K_F\right) + \frac{1}{n}\log\left(C_e\right) \tag{16}$$

where K_F (ln mg^{1-n}/g) and n (dimensionless) are experimental constants [29]. The Freundlich isotherm allows us to plot lnq_e as a function of lnC_e as shown in Fig. 17.

Table 4
The values of thermodynamic quantities

Settings	T (K)	$\Delta G°$ (kJ/mol)	$\Delta H°$ (kJ/mol)	$\Delta S°$ (J/mol)
Values	293	0.35305	–8.21941	–28.997
	323	4.936116		
	333	5.160884		
	338	5.758561		
	348	6.130786		

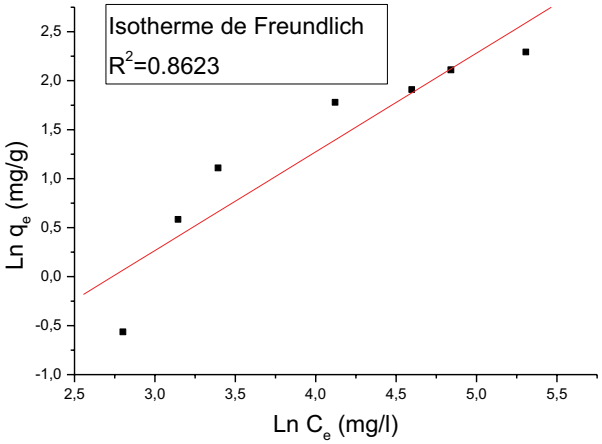

Fig. 17. Freundlich isotherm model.

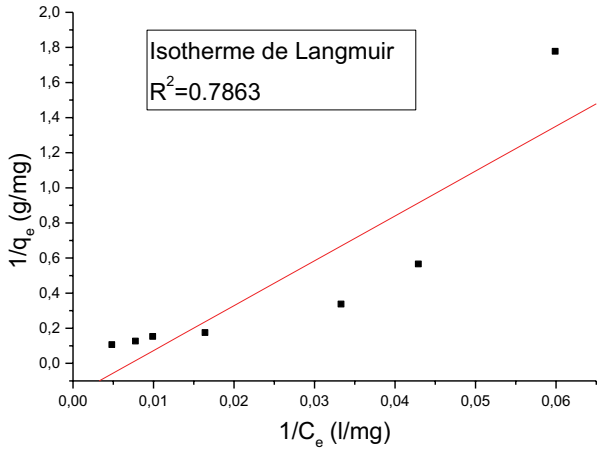

Fig. 18. Langmuir isotherm model.

3.5.2. Langmuir isotherm

Fig. 18 shows the variation of $1/q_e$ as a function of $1/C_e$ which signifies the Langmuir model. The linear form of the Langmuir isotherm [21]:

$$\frac{1}{q_e} = \frac{1}{C_e}\frac{1}{q_m K_L} + \frac{1}{q_m} \tag{17}$$

where K_L: equilibrium constant of Langmuir L/mg, q_e·q_m: quantity adsorbed at equilibrium and maximum successively mg/g.

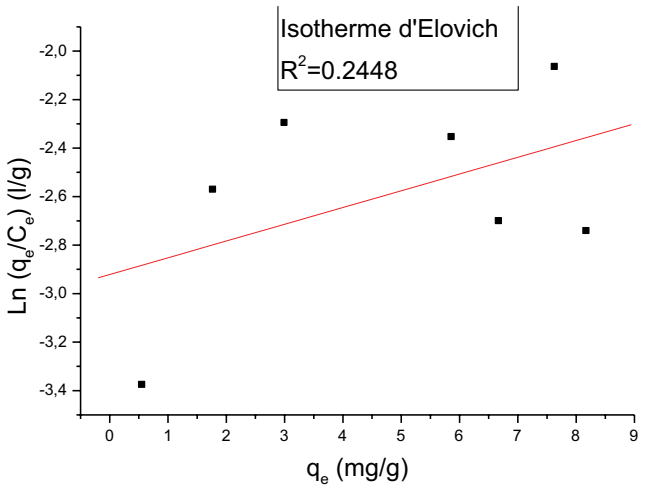

Fig. 19. Model of Elovich isotherm.

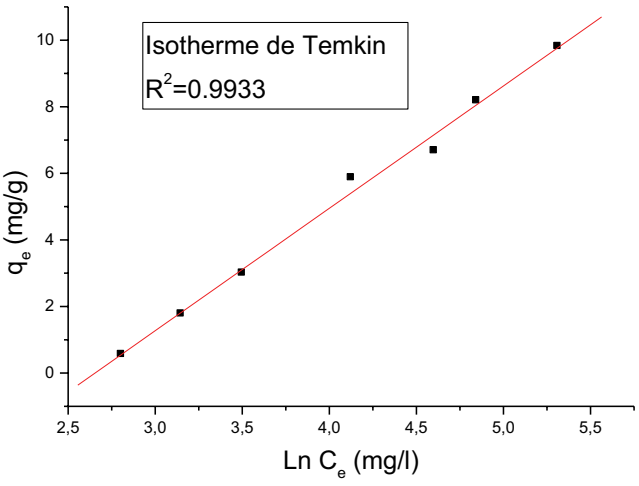

Fig. 20. Temkin's isotherm model.

3.5.3. Isotherm of Elovich

It is expressed by the following relationship:

$$\frac{q_e}{q_m} = \theta = K_E C_e \exp{-\left(\frac{q_e}{q_m}\right)} \tag{18}$$

where K_E, Elovich constant (in L/mg) [5] Elovich isotherm means a simple plot of $\ln(q_e/C_e)$ as a function of $\ln q$ as shown in Fig. 19.

3.5.4. Temkin isotherm

Plotting q_e or q as a function of $\ln C_e$ according to the following expression [8] and as shown in Fig. 20:

$$\frac{q_e}{q_m} = \theta = \frac{RT}{\Delta Q}\ln\left(K_T C_e\right) \tag{19}$$

where R = 8.314 J/mol K; T, absolute temperature (in K); ΔQ, adsorption energy variation (J/mol); K_T, Temkin constant (in L/mg).

3.5.5. Isotherm of Dubinin–Radushkevich

The Dubinin–Radushkevich isotherm is given by the following equation:

$$\ln q_e = \ln q_{m\mathrm{DR}} - K_D \varepsilon^2 \tag{20}$$

where $q_{m\mathrm{DR}}$ the maximum adsorption capacity in the micropores, K_D the constant related to the adsorption energy [5]. We plotted $\ln q_e$ as a function of ε^2 according to the Dubinin–Radushkevich model as Fig. 21.

3.5.6. Isotherm of Kiselev

The following relationship gives the Kiselev equation, known as the localized monolayer adsorption isotherm equation. The Kiselev equation can be expressed as:

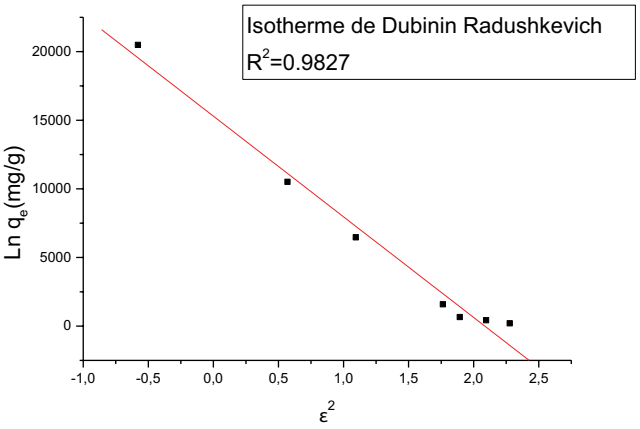

Fig. 21. Dubinin–Radushkevich isotherm model.

$$\frac{1}{C_e\left(1-\theta\right)} = \frac{K_1}{\theta} + K_1 k_n \tag{21}$$

where k_1: equilibrium constant of the adsorbate–adsorbent interaction; k_n: equilibrium constant of complex formation between neighboring molecules [30].

The Kiselev isotherm allows to plot the equilibrium constant as a function of x = as shown in Fig. 22.

3.5.7. Isotherm of Fowler–Guggenheim

The Fowler–Guggenheim equation assumes that the amount adsorbed at saturation q_m and the interaction energy W are independent of temperature. One can also express the equation in the form [30]:

$$\ln\frac{C_e\left(1-\theta\right)}{\theta} = -\ln K_{\mathrm{FG}} + \frac{2\theta W}{RT} \tag{22}$$

where W: interaction energy; K_{FG}: temperature dependent constant the Fowler–Guggenheim isotherm allows to plot as a function of (Fig. 23).

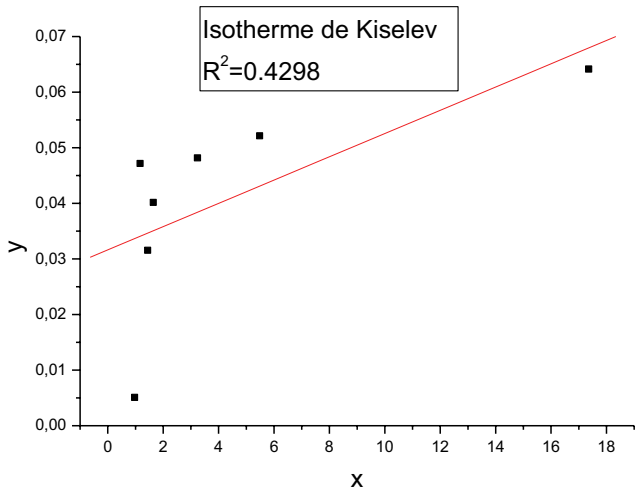

Fig. 22. Model of Kiselev isotherm.

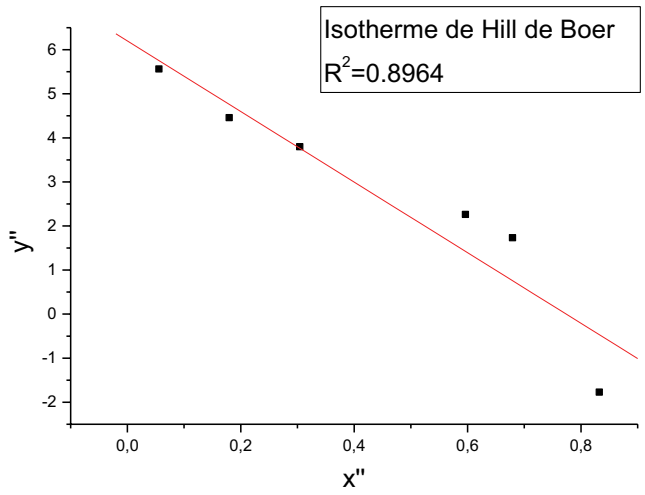

Fig. 24. Model of Boer's Hill.

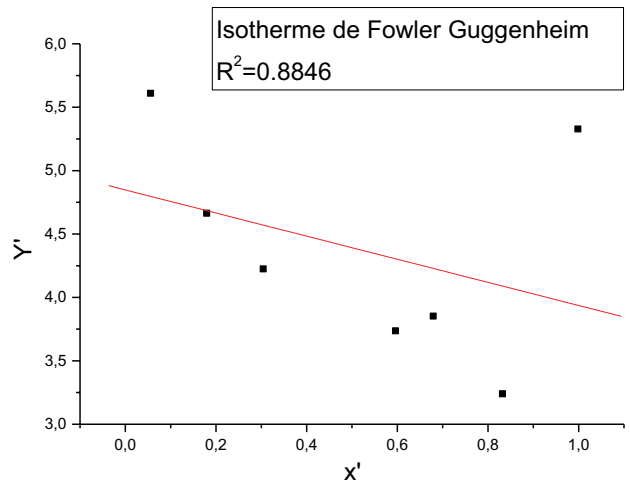

Fig. 23. Model of Fowler–Guggenheim isotherm.

3.5.8. Isotherm of Boer's Hill

These two authors have adopted an equation type of state van der Waals type equation of state to develop an adsorption isotherm equation, which takes into account the interactions and mobility of the adsorbed phase assumed to be delocalized.

$$\ln\frac{C_e(1-\theta)}{\theta}-\frac{\theta}{1-\theta}=-\ln k_1-\frac{k_2\theta}{RT} \tag{23}$$

where k_1: constant which represents the adsorbate–adsorbent interactions; k_2: is the interaction constant between adsorbates [30].

The Hill de Boer isotherm allows to plot as a function of as shown in Fig. 24.

Boer's Hill isotherm model The linear representations of the experimental values of this adsorption process allowed us to determine the equilibrium parameters and the values of the constants of each type of isotherms calculated by linear regression (Table 5).

From the modeling results of the adsorption isotherms grouped in Table 5, we observed that most of the linear models represent well the adsorption isotherms of phenol on prepared activated carbon with non-negligible correlation coefficients. The values of the regression coefficients indicate that the adsorption process of phenol by the olive kernel activated carbon is described favorably by the Temkin isotherm (with excellent linear regression coefficients (R^2 = 0.9933) which is very close to unity. Temkin's model shows that the heat of adsorption due to interactions with the adsorbate decreases linearly with the recovery rate [22]. The value of the energy obtained by the Temkin isotherm for the adsorption of phenol by activated carbon studied is lower than 40 kJ/mol indicating physisorption as the dominant type of adsorption. Indeed, the value of the regression coefficient shows that the Dubinin–Radushkevich model (R^2 = 0.9827) is adequate for a good description of this adsorption of phenol on the synthesized activated carbon. Due to the fact that the regression coefficients were not satisfactory for the Elovich and Kiselev isotherm, therefore they do not model our isotherm of phenol adsorption on the prepared activated carbon.

4. Conclusion

The study carried out in this work concerns the carbonization and then material activation of hard vegetable origin; the olive stones; to transform it into activated carbon, and then use it for the adsorption of organic pollutants including phenol. The experimental study conducted from all the results obtained, it is evident that the processes, carbonization, activation, and use of different activating agents are effective because our activated carbon has important properties according to their characterizations by ash content, moisture content, iodine index and Fourier transform infrared spectroscopy. The results FTIR analysis of prepared activated carbon revealed different oxygenated groups beside the carbonic structures of aromatic, aliphatic and carboxyl origin. The iodine value found of the synthesized activated carbon is quite high (>950 mg/g).

Table 5
Isotherm constants models

Models isotherms	Constants	Prepared activated carbon
Isotherm of Freundlich	K_F (mg/g)(L/mg)	0.0645
	n	1.0075
	R^2	0.8663
Langmuir isotherm	K_L (L/mg)	0.00678
	q_m (mg/g)	5.804
	R^2	0.7853
Isotherm of Elovich	q_m (mg/g)	–14.471
	K_E (L/mg)	–0.0037
	R^2	0.2448
Temkin isotherm	B_T (kJ/mol)	3.6767
	K_T (L/mol)	0.0703
	ΔQ (J/mol)	6.4981
	R^2	0.9933
Isotherm of Dubinin–Radushkevich	K_D (mol/j^2)	7335.8
	R^2	0.9827
Isotherm of Kiselev	k_1 (L/mg)	0.0021
	k_n (L/mg)	15.048
	R^2	0.4298
Isotherm of Fowler–Guggenheim	K_{FG} (L/mg)	0.00047
	W (kJ/mol)	–3.1079
	R^2	0.8846
Isotherm of Boer's Hill	k_1 (L/mg)	0.00247
	k_2 (kJ/mol)	19503.2
	R^2	0.8964

A series of experiments was then carried out to study the influence of some parameters on the adsorption capacity of phenol by prepared activated carbon such as adsorbent mass, contact time, pH, temperature and initial phenol concentration. The adsorption capacity of phenol increases with the increase of the adsorbent mass, however, it decreases when the pH of the phenol solution decreases. It is noticeable that an acid pH has a favorable effect on the adsorption process of phenol by carbon.

All the obtained results show that the kinetics of adsorption of phenol on the prepared activated carbon is well described by the pseudo-second-order model with a correlation coefficient close to the unit $R^2 = 0.9928$ and the value of the calculated adsorbed quantity is very close to the value of experimental adsorbed quantity. The modeling of the phenol adsorption isotherms obtained, agrees well with the Temkin model for prepared activated carbon (with excellent linear regression coefficient ($R^2 = 0.9933$) which is very close to unity), and the Temkin energy highlights an exothermic adsorption. The thermodynamic study revealed that the adsorption is nonspecific and exothermic, and the examination of the standard enthalpy value of the adsorption (<40 kJ/mol) shows that it is a physisorption. It is important to point out at the end of this study that the exploitation of this kind of materials is very interesting from the economic point of view in the water decontamination.

References

[1] N. Bouchemal, Z. Merzougui, F. Addoun, Adsorption in aqueous media of two-dyes on activated carbon based on date nuclei, J. Algerian Chem. Soc., 21 (2011) 1–14.

[2] E. Fernandez Ibañez, Study of Carbonization and Activation of Hard and Soft Plant Precursors, Ph.D. Thesis, University of NEUCHÂTEL, 2002.

[3] A.K.K. Mayeko, P. Nokivesituluta, J. Di Phanzu, D.W.M.G.E. Bakambo, B.I. Lopaka, J.M. Mulangala, Adsorption of quinine dihydrochloride on inexpensive activated carbon based on sugar cane bagasse impregnated with phosphoric acid, Int. J. Biol. Chem. Sci., 6 (2012) 1337–1359.

[4] A. Nait-Merzoug, A. Benjaballah, O. Guellati, Preparation and characterization of an activated carbon based on agricultural waste, Int. J. Biol. Chem. Sci., 6 (2016) 461–478.

[5] K. Amel, Experimental Study of the Elimination of Organic and Inorganic Pollutants by Adsorption on Natural Materials: Application to Orange and Banana Peel, Doctoral Thesis, Mentouri of Constantine University, 2012.

[6] S.M. Beyan, S. Venkatesa Prabhu, T.A. Ambio, C. Gomadurai, A statistical modeling and optimization for Cr(VI) adsorption from aqueous media via teff straw-based activated carbon: isotherm, kinetics, and thermodynamic studies, Adsorpt. Sci. Technol., 2022 (2022) 7998069, doi: 10.1155/2022/7998069.

[7] A.E. Armand, Y.Y. Augustin, K.Y. Urbain, T. Albert, Optimization of the preparation of activated carbon based on corn cobs and physico-chemical characterization, Int. J. Innovation Appl. Stud., 29 (2020) 1161–1171.

[8] B. Rabia, Comparative Study of the Elimination of Textile Dyes by Two Adsorbents: Natural and Active, Ph.D. Thesis, University of Djilali liabes – Sidi Bel Abbes, 2021.

[9] N.M. Haimour, S. Emeish, Utilisation of date stones for production of activated carbon using phosphoric acid, Waste Manage., 26 (2006) 651–660.

[10] T.A. Amibo, S.M. Beyan, T.M. Damite, Production and optimization of bio-based silica nanoparticle from teff straw (*Eragrostis tef*) using RSM-based modeling, characterization aspects, and adsorption efficacy of Methyl orange dye, J. Chem., 2022 (2022) 9770520, doi: 10.1155/2022/9770520.

[11] T. Bohli, A. Ouederni, N. Fiol, I. Villaescusa, Evaluation of an activated carbon from olive stones used as an adsorbent for heavy metal removal from aqueous phases, C.R. Chim., 18 (2015) 88–99.

[12] O. Üner, Ü. Geçgel, Y. Bayrak, Preparation and characterization of mesoporous activated carbons from waste watermelon rind by using the chemical activation method with zinc chloride, Arabian J. Chem., 12 (2019) 3621–3627.

[13] R. Boudia, G. Mimanne, K. Benhabib, L. Pirault-Roy, Preparation of mesoporous activated carbon from date stones for the adsorption of Bemacid red, Water Science Technol., 79 (2019) 1357–1366.

[14] I. Tchakala, L. Moctar Bawa, G. Djaneye-Boundjou, K.S. Doni, P Nambo, Optimization of the Process for Preparing Activated Carbon by Chemical Means (H_3PO_4) from Shea Cake and Cottonseed Cake, Third International Conference on Energy, Materials, Applied Energetics and Pollution ICEMAEP, 2012.

[15] I.-H.T. Kuete, D.R. Tchuifon, G.N. Ndifor-Angwafor, A.T. Kamdem, S.G. Anagho, Kinetic, isotherm and thermodynamic studies of the adsorption of Thymol blue onto powdered activated carbons from *Garcinia cola* nut shells impregnated with H_3PO_4 and KOH: non-linear regression analysis, J. Encapsulation Adsorpt. Sci., 10 (2020), doi: 10.4236/jeas.2020.101001.

[16] A. Hamouche, Kinetic and Thermodynamic Study of the Adsorption of Heavy Metals by the Use of Natural Adsorbents, University Doctoral Thesis Mohammed Bougara Boumerdes, 2013.

[17] Y. Asrat, A.T. Adugna, M. Kamaraj, S.M. Beyan, Adsorption phenomenon of *Arundinaria alpina* stem-based activated carbon for the removal of lead from aqueous solution, J. Chem., 2021 (2021) 5554353, doi: 10.1155/2021/5554353.

[18] C. Noura, Use of Date Palm By-Products in the Physico-Chemical Treatment of Polluted Water, University Ph.D. Thesis HADJ LAKHDAR – BATNA, 2014.
[19] D. Ouattara Kra, G.P. Atheba, N'da Arsène Kouadio, P. Drogui, A. Trokourey, Activated carbon based on acacia wood (*Auriculeaformis*, Côte d'Ivoire) and application to the environment through the elimination of Pb^{2+} ions in industrial effluents, J. Encapsulation Adsorpt. Sci., 11 (2021) 18–43.
[20] M. Soriya, Synthesis, Characterization of Functionalized Activated Carbons and Study of Their Applications in the Elimination of Pollutants, Ph.D. Thesis of University Mohamed Boudiaf - M'sila, 2021.
[21] El Hadji M.R. Gadji, C. Kane, M. N'doye, M.K. Mbacke, M. Faye, P.G. Faye, P. Mendy, C.M. Diop, Kinetic and thermodynamic study of the adsorption of fluorine in aqueous solution on calcined bones, Int. J. Innov. Sci. Res., 38 (2018) 30–43.
[22] M. Goussem, Adsorption of an Organic Surfactant DBSA Compound on a Geomaterial Obtained by Combining a Calcium Clay and An Activated Carbon, Doctoral Thesis, University Djillali Liabes, 2012.
[23] A. Aarfane, A. Salhi, M. El Krati, S. Tahiri, M. Monkade, E.K. Lhadi, M. Bensitel, Kinetic and thermodynamic study of the adsorption of Red195 and methylene blue dyes in aqueous media on fly ash and bottom ash, J. Mater. Environ. Sci., 5 (2014) 1927–1939.
[24] A.Q. Alorabi, Effective removal of malachite green from aqueous solutions using magnetic nanocomposite: synthesis, characterization, and equilibrium study, Adsorpt. Sci. Technol., 2021 (2021) 2359110, doi: 10.1155/2021/2359110.
[25] L. Bacha, L. Aichiou, M. Bourouina, Kinetic and Thermodynamic Study of NET Adsorption Process on Clay and Modeling for a Response Surface, Université Abderrahmane Mira, 2017.
[26] N. Gherbi, Doctoral Thesis, Faculty of Engineering Sciences, Department of Industrial Chemistry, Ph.D. Thesis From the University of Constantine, Algeria, 2008.
[27] A. Sarı, M. Tuzen, Kinetic and equilibrium studies of biosorption of Pb(II) and Cd(II) from Aqueous Solution by macrofungus (*Amanita rubescens*) biomass, J. Hazard. Mater., 164 (2009) 1004–1011.
[28] L. Liu, Y. Rao, C. Tian, T. Huang, J. Lu, M. Zhang, M. Han, Adsorption performance of La(III) and Y(III) on orange peel: impact of experimental variables, isotherms, and kinetics, Adsorpt. Sci. Technol., 2021 (2021) 7189639, doi: 10.1155/2021/7189639.
[29] K. Philip, R. Jacob, J. Gopalakrishnan, Characterization of cassava root husk powder: equilibrium, kinetic and modeling studies as bioadsorbent for copper(II) and lead(II), J. Encapsulation Adsorpt. Sci., 11 (2021) 69–86.
[30] M. Zarrouki, Study of Adsorption in a Liquid–Solid System: Solution of Dicyanoaurate-Activated Carbon Ion, National School of Mines of Saint-Etienne, 1990. French 1990INPG4201, 2013.